LASER INTERFEROMETER GRAVITATIONAL WAVE OBSERVATORY
- LIGO -
CALIFORNIA INSTITUTE OF TECHNOLOGY
MASSACHUSETTS INSTITUTE OF TECHNOLOGY

Technical Note	**LIGO-T1800224–v0**	2018/06/30

Scattered Light Study of Advanced LIGO in Observation Run 2 - Interim Report 1 -

SURF Students: Wenxuan Jia, Mentor: Anamaria Effler, Valery Frolov

California Institute of Technology
LIGO Project, MS 18-34
Pasadena, CA 91125
Phone (626) 395-2129
Fax (626) 304-9834
E-mail: info@ligo.caltech.edu

Massachusetts Institute of Technology
LIGO Project, Room NW22-295
Cambridge, MA 02139
Phone (617) 253-4824
Fax (617) 253-7014
E-mail: info@ligo.mit.edu

LIGO Hanford Observatory
Route 10, Mile Marker 2
Richland, WA 99352
Phone (509) 372-8106
Fax (509) 372-8137
E-mail: info@ligo.caltech.edu

LIGO Livingston Observatory
19100 LIGO Lane
Livingston, LA 70754
Phone (225) 686-3100
Fax (225) 686-7189
E-mail: info@ligo.caltech.edu

http://www.ligo.caltech.edu/

1 Introduction

In the dual-recycled Michelson interferometer in Advanced LIGO, the scattered light in the resonant cavity, for example the low-angle scatter caused by unevenness of the high-reflection (HR) surface of the test mass, generates noise to the differential arm (DARM) signal that contains the gravitational wave (GW) information [1]. The impact of the scattered light is demonstrated on the noise budget diagram, as shown in Figure 1. The difference between the

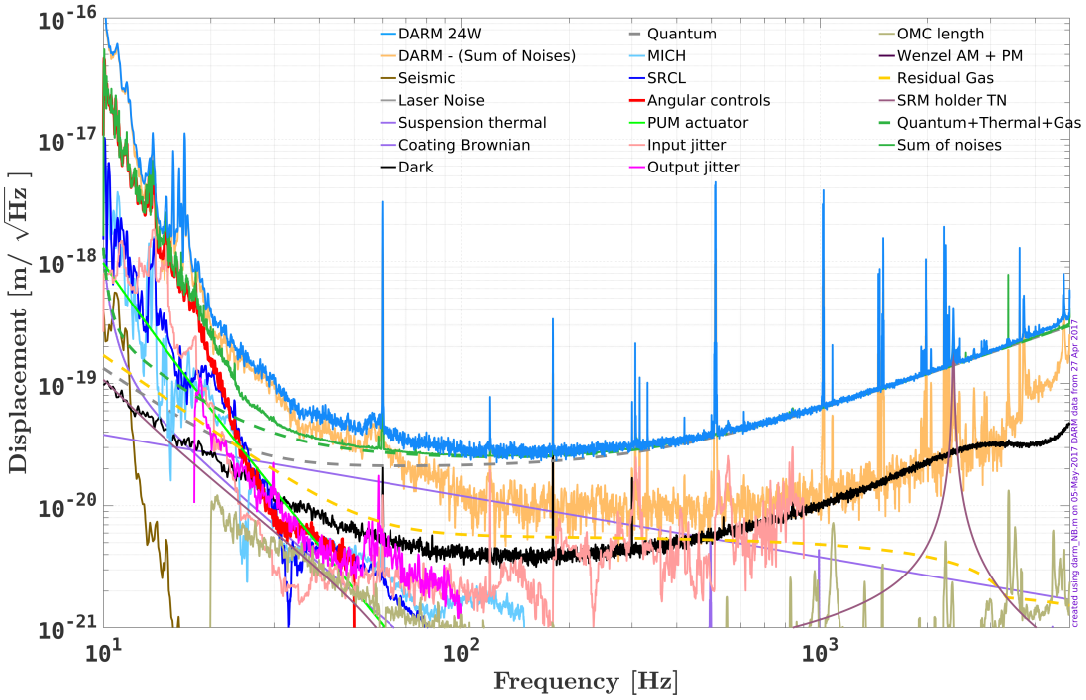

Figure 1: Noise budget of LIGO Livingston Observatory on Apr. 27, 2017. The blue curve 'DARM 24W' in the diagram represents the DARM signal sensitivity, and the solid green curve 'Sum of noises' is the sum of theoretical noise budgets from all sources in the legend. (Credit: Anamaria Effler [2])

current sensitivity and noise budget at low frequencies (around 20 Hz) is partly attributed to the scattered light [3]. In this project, we aim at understanding the data measurements of scatter and exploring applications with such information.

The low-angle scatter in the Fabry-Perot (FP) cavity is measured by photodiodes (PD) mounted on the baffle and compared with the Static Interferometer Simulation (SIS) modeling, which is a FFT-based computation tool that simulates field propagation in the resonant cavity and accounts for user-defined HR profile on the test masses [4]. The couplings between scatter with other physical quantities in Observation Run 2, for example main beam position and time, are also investigated to provide fundamentals for future applications.

2 Materials & Methods

2.1 FP cavity scatter measurement

To prevent scattered photons from re-entering the main beam of interferometer, multiple light baffles are mounted on beam paths as shown in Figure 2. Those beamtube baffles

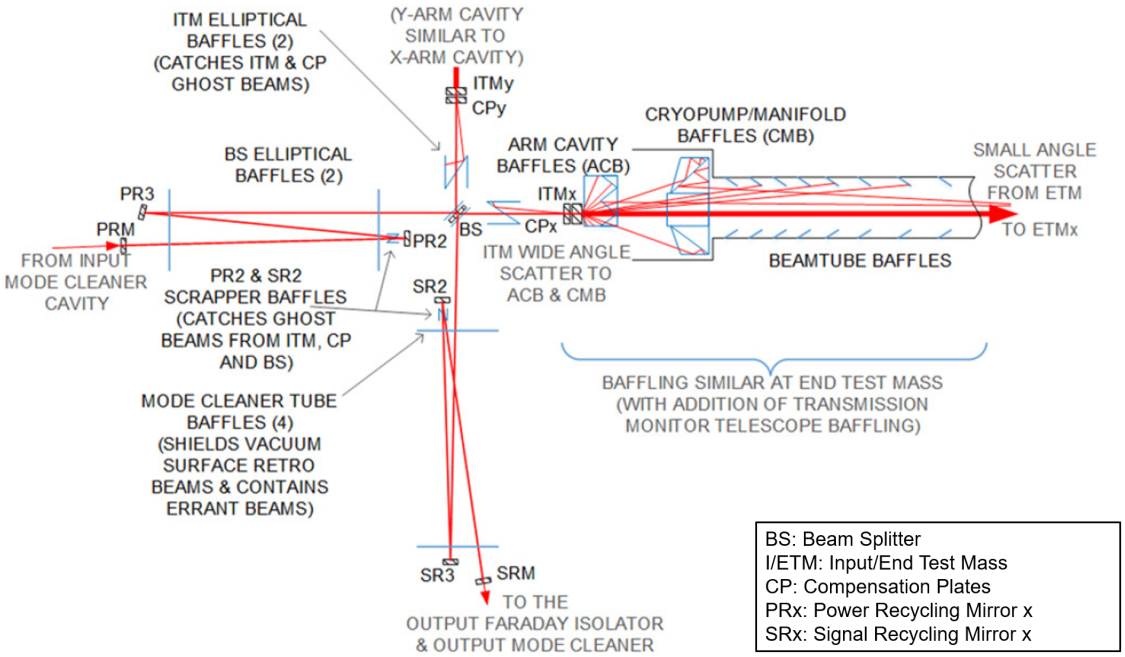

Figure 2: Locations of scattered light baffles in the LIGO optical configuration [5].

mounted on the sidewalls of the ultra-high vacuum cavity as well as the cryopump/manifold baffles are meant to block the large-angle scatter. The low-angle scatter from the far test mass (4 km away) is caught by the arm cavity baffle (abbreviated as baffle) placed in front of each test mass optic [5]. There are four *Excelitas YAG-444-AH* photodiodes mounted on each baffle of the test mass to measure the intensity of low-angle scattered light from the test mass on the other side of FP cavity. The configurations of PD are pictured in Figure 3.

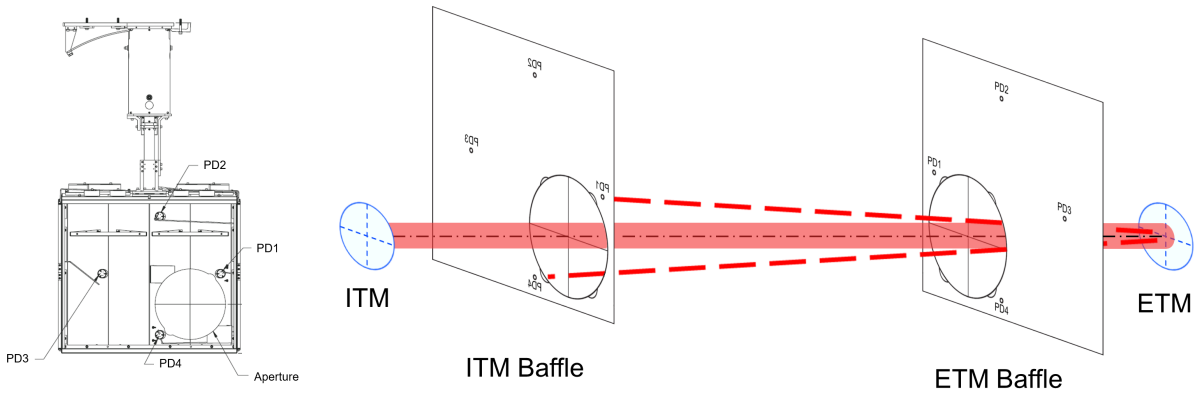

(a) (b)

Figure 3: Schematics of the baffle PD measuring low-angle scatter. (a) the back view of the baffle with four PDs mounted (Note that PD 1 and 4 are closer to aperture than Pd 2 and 3. Credit: Jose Chavez [6]). (b) FP cavity with sample ETM scatter caught on ITM baffle PD 1 and 4. The shaded line is resonant main beam and the scatter paths are annotated in dashed lines. The length of the cavity is shortened and not to scale.

In the Observation run 2 (O2) from Nov. 30, 2016 to Aug. 25, 2017, all of the 16 PDs mounted on 4 baffles have measured the scatter intensity with sampling frequency of 16 Hz, and the raw data can be accessed by channels *L1:AOS-I(E)TMX(Y)_BAFFLEPD_1(2,3,4)_POWER*. The variance across photodiodes on the same baffle are calibrated to ensure valid comparison of scatter power measured by them.

2.2 Calibration of low-angle scatter measurements (PD 1 and 4)

During the O2, the test masses in the FP cavity was occasionally misaligned from facing to each other and failed to form resonance. The main beam was then centered back to the correct position by yawing or pitching the test masses. To determine the correct yaw & pitch gains of ETM, the green laser (532 nm) located at the back of ETM was directed to the PD 1 and 4 on ITM baffle respectively by changing ETM attitude, and then the average of the separate gains would center the main beam on ITM (Figure 4 (a)). Similarly, the ITM yaw & pitch can be determined by averaging gains that point laser beam at the PD 1 and 4 of ETM baffle, as shown in Figure 4 (b). The PD 1 and 4 measurements during beam centering can be used to find the variance between them.

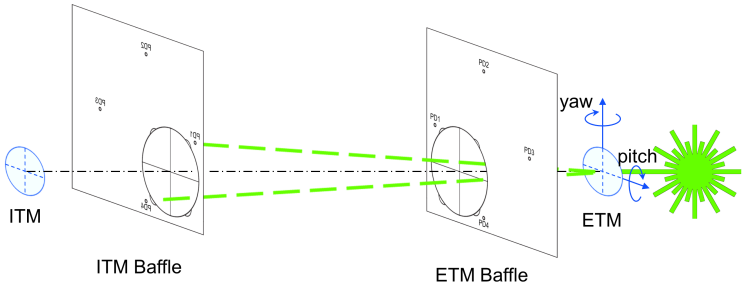

(a) Centering main beam on ITM by ETM yaw & pitch

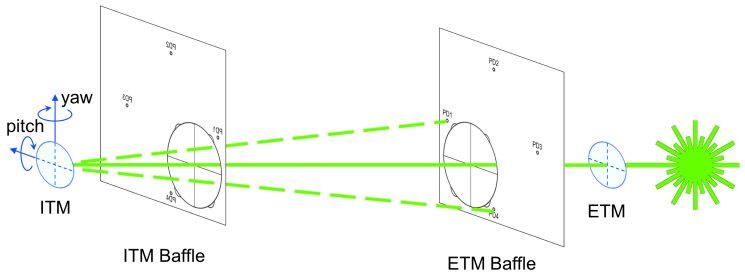

(b) Centering main beam on ETM by ITM yaw & pitch

Figure 4: Schematics of the beam centering process, during which the PD 1 and 4 are shined directly by the same source

The beam centering process can be found when *L1:GRD-ISC_LOCK_STATE_N* equals to 9. The raw data of PD 1 and 4 measurements at the first three and last three times of centering process through O2 are found to compute the variance, an example of ITMX PD as shown in Figure 5.

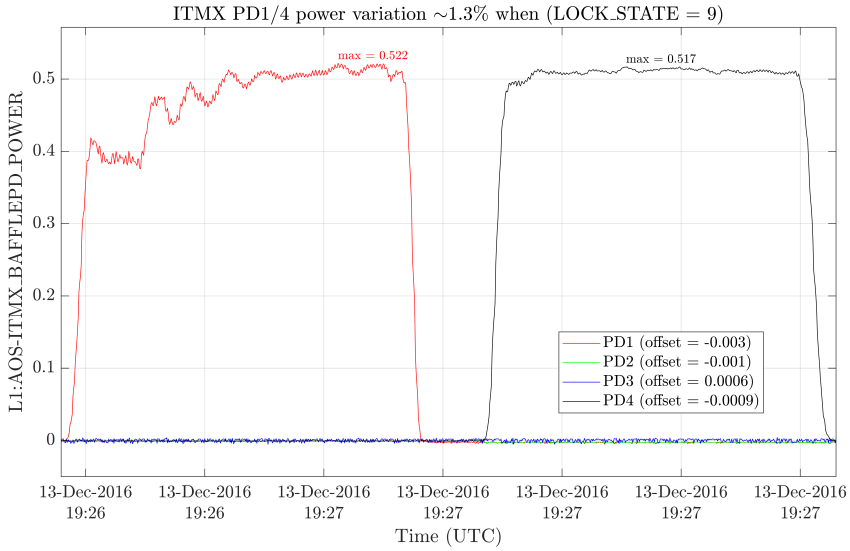

Figure 5: Time series of ITMX baffle PD 1 and 4 measurements during the first beam centering. Each grid is 10 seconds,

It is seen that the PD 1 was under green beam for 20 seconds until its power reaches maximum, and then it was repeated on PD 4. In contrast, the other two PD (2 and 3) were not receiving any light and stayed null. The calibration results for all baffles during the six beam centering processes are summarized in Table 1.

Table 1: Variance of PD 1 and 4 on all arm cavity baffles measured at first and last three times of main beam centering

Time	ITMX	ETMX	ITMY	ETMY
Dec. 13, 2016	1.3%	2.1%	2.9%	0.9%
Dec. 19, 2016	3.7%	1.9%	1.1%	1.0%
Dec. 21, 2016	4.1%	2.2%	0.9%	1.6%
Jul. 31, 2017	4.0%	2.0%	2.5%	0.9%
Aug. 5, 2017	4.1%	2.0%	3.4%	1.1%
Aug. 22, 2017	4.4%	1.8%	2.0%	0.8%

The variance of PD 1 and PD 4 at all baffles can be concluded as $2\% \pm 1\%$. Assume that the response of PD is the same for both green and IR laser (1064 nm), the variance of PD 1 and 4 is negligible and much less than the uncertainties caused by fluctuating environmental effects.

3 Preliminary Results

3.1 Scatter change through O2

The dual-recycled Michelson interferometer is most sensitive to gravitational wave ripples in space-time when all of its cavities are locked in resonance. However, various external factors caused the detector to fail maintaining the desired locked state in O2, during which the PD data is not measuring the scatter of the full power of main beam. Even in the low-noise mode, the interferometer may be under other tests instead of observing GW. These periods are not interesting to us, and we eliminate the PD measurement data in these disturbed time intervals. In addition, the scatter is also susceptible to changes in the beam positions caused by changes of test mass attitude. Therefore, the PD data needs to be filtered such that they are measuring the scatter during stable observing period (science-run mode). Table 2 summarizes known factors that affect scatter in O2 and their channel names.

Table 2: Known factors that couple with low-angle scatter in FP cavity

Factors	Channel names
Locked state	*L1:GRD-ISC_LOCK_STATE_N*
Science-run mode	*L1:ODC-OPERATOR_OBSERVATION_READY*
Power	*L1:IMC-PWR_IN_OUTPUT* *L1:LSC-PRC_GAIN_MON*
Test mass attitude	*L1:SUS-I(E)TMX(Y)_L2_DRIVEALIGN_P(Y)2L_GAIN*
PR2 attitude	*L1:SUS-PR2_M3_DRIVEALIGN_P(Y)2L_GAIN*

For each locked state, its transient response is filtered by removing the first and last 1 hour of data in its period. The transience filter of 1 hour is also applied to periods when all *DRIVEALIGN* gains are constant. The resulting PD data through entire O2 is presented in Figure 6.

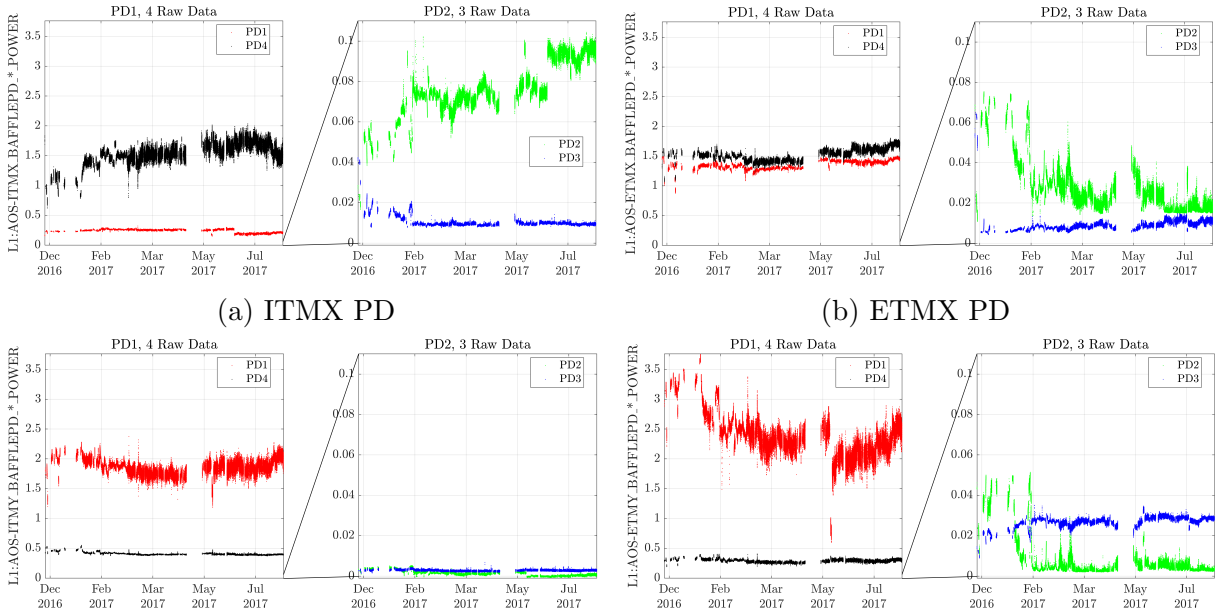

(a) ITMX PD (b) ETMX PD

(c) ITMY PD (d) ETMY PD

Figure 6: Filtered PD minute-trend data on all arm cavity baffles throughout O2.

Since the PD 1 and 4 are closer to the main beam than PD 2 and 3, they receive higher scatter intensity. The entire minute-trend data throughout O2 is considered stable, and the fluctuations of the measurements could be caused by unsteady environmental factors listed in Table 2, whose minute-trend data is presented as follows.

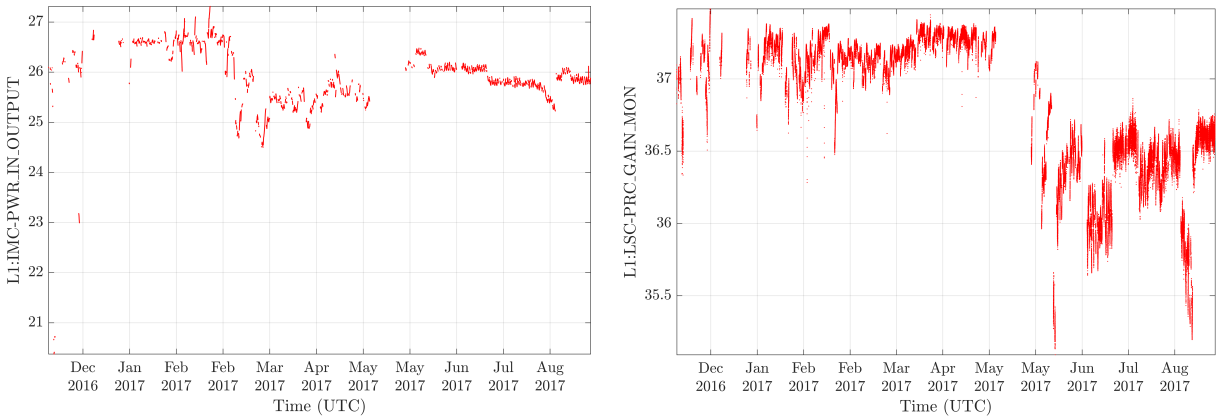

(a) Laser power input (b) Power recycling gain

Figure 7: Cavity power minute-trend data throughout O2.

Since the variations of the majority of laser power gain is within 10% and that of power recycling gain is within 5%, we can assume first-order coupling between power and scatter. The scatter data is normalized by dividing it with cavity power $(laserpower)(PRG)/2$. The spot position setting of PR2 remains constant for all the filtered periods of O2, thus its coupling with scatter can be ignored. The total eight yaw & pitch gains for four test masses are constant only for certain period in the O2, which implies that the entire O2 data needs to be sectioned with periods when all test masses are stable. There are 366 sections found in O2 when the following criteria are satisfied simultaneously:

1. The cavity is locked for more than 3 hours (first and last 1 hour transience are filtered)
2. All yaw & pitch gains are constant for more than 3 hours (transience will be filtered)
3. The variation of laser power input is less than 1 W
4. The variation of recycling gain is less than 1

The time periods for constant yaw & pitch gains are summarized in Table 3

Table 3: Stable drive align gains in O2. The start date for each row of gains is in the leftmost column of that row

	ITMXyaw	ITMXpitch	ETMXyaw	ETMXpitch	ITMYyaw	ITMYpitch	ETMYyaw	ETMYpitch
30-Nov-2016:	-1.70	0.00	0.60	1.40	0.40	0.20	-0.10	1.70
07-Dec-2016:	-1.70	0.00	-0.50	1.40	0.40	0.20	-0.10	1.70
14-Dec-2016:	-1.70	0.00	-1.00	1.40	0.40	0.20	-0.10	1.70
15-Dec-2016:	-1.70	0.00	-0.50	1.40	0.40	0.20	-0.10	1.70
23-Jan-2017:	-2.09	-0.05	-0.50	1.40	0.70	0.15	-0.10	1.70
17-Feb-2017:	-2.00	-0.05	-0.50	1.40	0.70	0.15	-0.10	1.70
25-Feb-2017:	-2.00	-0.05	-0.50	1.40	0.40	0.20	-0.10	1.70
06-Jun-2017:	-2.00	-0.05	-0.50	0.70	0.40	0.20	-0.10	0.70
08-Jun-2017:	-2.00	-0.05	-0.50	1.40	0.40	0.20	-0.10	1.40
02-Jul-2017:	-2.00	-0.05	-0.50	0.70	0.40	0.20	-0.10	1.40
02-Aug-2017:	-1.70	-0.05	-0.50	0.70	0.40	-0.20	-0.10	1.40
03-Aug-2017:	-2.00	-0.05	-0.50	0.70	0.40	-0.20	-0.10	1.40
04-Aug-2017:	-2.00	-0.05	-0.50	0.70	0.40	0.20	-0.10	1.40

It is seen that the longest period in Table 3 is from Feb. 24, 2017 to Jun. 08, 2017. Therefore, the time series of raw PD data is obtained for all sections in this period, and its average and uncertainty (standard deviation) is computed and presented in Figure 8

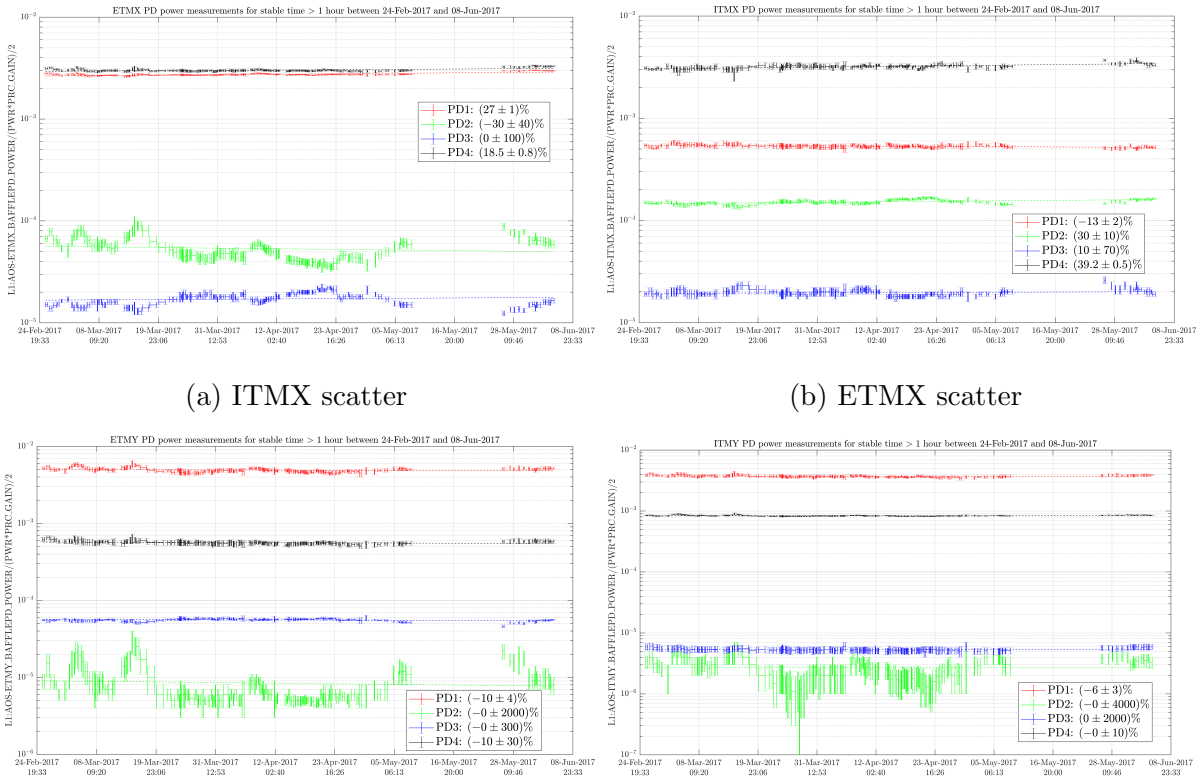

(a) ITMX scatter

(b) ETMX scatter

(c) ITMY scatter

(d) ETMY scatter

Figure 8: Trend of scatter measured on all sections from Feb. 24, 2017 to Jun. 08, 2017

Line fitting is done on each trend data, and their slopes are used to estimate overall change of scatter power, which is presented in the legend of each graph. Since the PD 2 and 3 measure relatively small scatter, their data is more unsteady and leads to large uncertainties like $0\% \pm 2000\%$ measured by ITMY PD 3. Overall, it is difficult to summarize an unified trend for all PD measurements and conclude for scatter change over O2, as some scatter reveals growth and yet other shows decay. We would integrate all of data from all period sections by normalizing them with respect to beam positions based on simulation like SIS such that the trend of entire O2 can be estimated.

3.2 Comparison between scatter measurements and SIS

In Figure 6 of the PD data for the entire O2, the variations of PD 1 and 4 on ITMX, ITMY and ETMY baffle are abnormally large (around the factor of 10), given their symmetrical positioning relative to the aperture. calibration is not the reason as indicated in section 2.2. Thus, the SIS tool is resorted to explain such difference. The configuration of simulation is mostly adapted from Hunter's work [7], except for his HR profile whose self-defined bumps and tilts are removed to center the beam on the aperture. The comparison of simulation result and scatter measurements in O2 are presented in Figure 9.

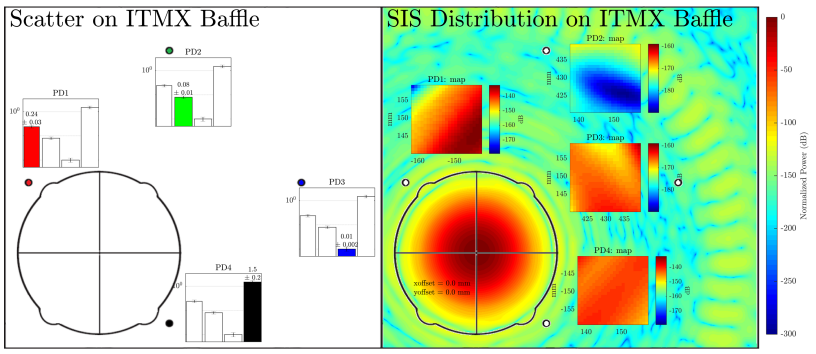

(a) ITMX PD measurements vs. SIS

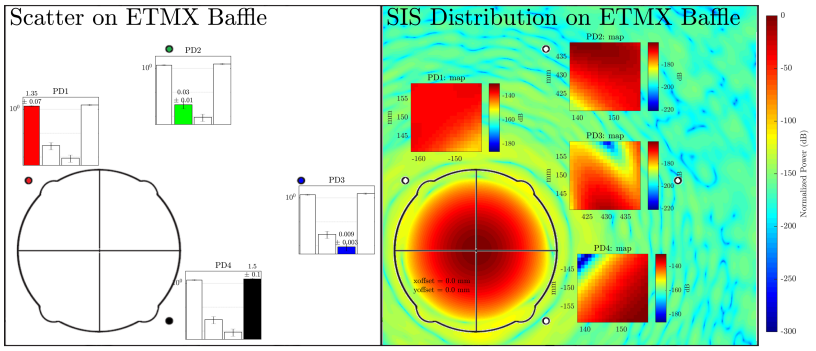

(b) ETMX PD measurements vs. SIS

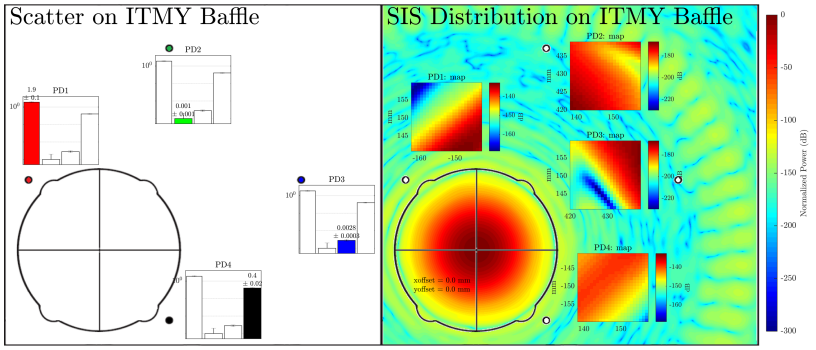

(c) ITMY PD measurements vs. SIS

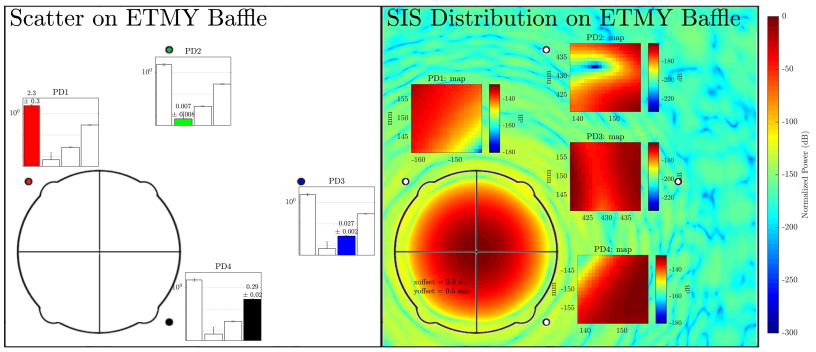

(d) ETMY PD measurements vs. SIS

Figure 9: Comparisons between actual scatter measurements (left) with SIS results (right). The subplots in the left figures are scatter power of that PD (highlighted) compared with others. The subplots in the right figure shows the zoomed-in power distribution of PD in the 2 cm square around it.

In the simulation plot, the position of PD 2 and 3 are next to the scattered light ripples, which may lead to the sudden rise of power measurements. However, the simulation map of scatter power on PD 1 and 4 do not reveal power change larger than one decade. The movement of the beam within 2 cm around the center of aperture does not lead to the change of power measurements on PD 1 and 4. It would be better to do radial integration of power on the PD to find the averaged result than referring to local distribution.

4 Next Work

The plan for the future work is listed as follows:

1. Direct calibration on baffle PD to find absolute scatter power distribution
2. Investigate the unsteadiness of PD measurements before Feb. 2017 (Figure 6)
3. Understand more about SIS from Dr. Yamamoto and integrate the latest modeling to the simulation. The change of distribution for different beam position will also be accounted.
4. Take advantage of transient response of the beam alignment to generate more data of coupling between beam position and scatter distribution on PD.

References

[1] P. Saulson, *Interferometric Gravitational Wave Detectors, 2nd Edition*. Section 6.6 pp. 99 (2017).

[2] A. Effler, *Latest noise budget*. LLO Logbook #33552 (2017).

[3] C. Austin, *Stray light control update*. LIGO-G1800466-v1 (2018).

[4] H. Yamamoto, *SIS (Stationary Interferometer Simulation) manual*. LIGO-T070039-v8.

[5] The LIGO Scientific Collaboration, *Advanced LIGO*. Class. Quantum Grav. 32 074001 (2015).

[6] J. Chavez and E. Sanchez, *AdvLIGO SUS BSC5-L1, XYZ Local CS for SLC Arm Cavity Baffle*. LIGO-D1200677-v1.

[7] H. Rew and J. Betzwieser, *Modeling of Optical Scattering in Advanced LIGO*. LIGO-P1400197.